🔓**Open Access**

Resonant Excitation Analysis on Asymmetrical Lateral Leakage of Light in Finite Zero-Contrast Grating Mirror
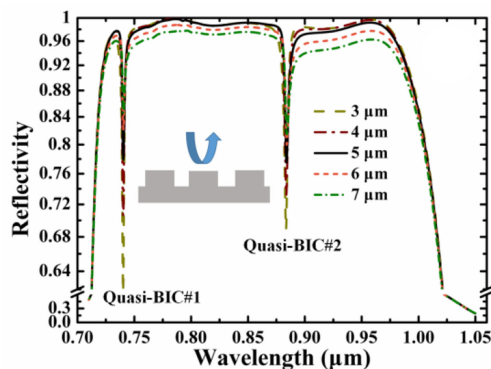
Tian Sang
Xin Yin
Honglong Qi
Jian Gao
Xinshang Niu
Hongfei Jiao

Resonant Excitation Analysis on Asymmetrical Lateral Leakage of Light in Finite Zero-Contrast Grating Mirror

Tian Sang ⓘ**,**[1] **Xin Yin,**[1] **Honglong Qi,**[1] **Jian Gao,**[1]
Xinshang Niu,[2] **and Hongfei Jiao**[2]

[1]Department of Photoelectric Information Science and Engineering, School of Science,
Jiangnan University, Wuxi 214122, China
[2]Key Laboratory of Advanced Micro-Structured Materials MOE Institute of Precision Optical
Engineering, School of Physics Science and Engineering, Tongji University, Shanghai
200092, China

Abstract: Resonant excitation analysis on asymmetrical lateral leakage of light in the finite zero-contrast grating (ZCG) mirror is demonstrated, and the size effect of the excited source is investigated. The dispersion equation of slab waveguide for the TM mode is proposed to evaluate the resonant condition of the ZCG mirror, and it is shown that the mirror effect of the infinite ZCG is resulted from the overlapping of order-mode resonance pairs. However, two leaky channels are excited in spectra of the finite ZCG mirror for the normal-incident Gaussian source, where bound states in the continuums (BICs) turn into quasi-BICs as the angular component is nonzero. The leaky channels are confined in the grating layer and the sublayer, and they are all transferred from the symmetrical mode to the asymmetrical mode along the lateral direction from the center of the ZCG. The asymmetrical loss of the lateral leakage of light relative to incidence direction, in principle, can break reflection reciprocity of the symmetrical system of the finite ZCG mirror. By changing the excited source from the grating side to the sublayer side, the lateral leakage of light of the finite ZCG mirror can be efficiently reduced.

Index Terms: Zero-contrast grating, asymmetrical lateral leakage, order-mode resonance, bound states in the continuums.

1. Introduction

Broadband mirrors with very high reflectivity are of great scientific and technological interest due to their versatile applications in optoelectronics. Generally, broadband mirrors can be realized by using metallic mirrors or dielectric mirrors. Metallic mirrors with broad reflection band are low in reflectivity due to their inherent absorption loss. Dielectric mirrors have negligible absorption loss, thus they can achieve high reflectivity. However, dielectric mirrors are generally composed of multilayer films, the reflection bands of dielectric mirrors are limited by the refractive index difference of the materials used, and the deposition methods are often not precise enough to achieve very high reflectivity [1], [2].
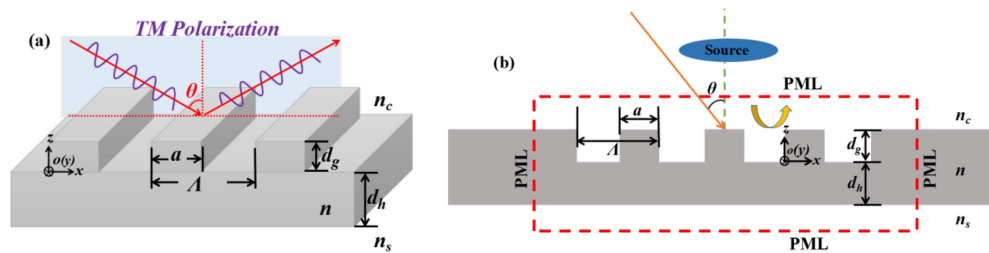
Fig. 1. (a) Schematic diagram of the infinite ZCG under the TM polarized plane wave illumination. (b) Calculation model of the finite ZCG.

High-contrast grating (HCG) is a single-layer near-wavelength grating with large refractive index difference from surrounding materials, and it can be functioned as a broadband mirror with very high reflectivity [3], [4]. This new type of mirror requires only about a half-wavelength thickness, but it can provide a high reflection band that is twice as that of the conventional all-semiconductor distributed Bragg reflector (DBR) [5], [6], which has significant importance in the applications such as vertical-cavity surface-emitting lasers (VCSELs) [7]–[9]. In practice, driven by chip-scale optical reflector and lab-on-chip sensing applications, it is becoming increasingly urgent to minimize the size of integrated photonic devices such as the subwavelength gratings [10]. In fact, there are many essential differences between the finite grating mirror and its infinite periodic counterpart. For example, it is shown that a finite HCG with guided mode can be functioned as optical sensor [11], and the mode splitting phenomenon can be observed [12]. In particular, high reflection band of the finite HCG is less broad as compared to the infinite case, and losses into a guided mode excited in the HCG plane are identified [13]. Recently, an alternative approach to obtain broadband reflection with very high reflectivity is proposed as zero-contrast grating (ZCG) [14], [15]. For this structure, the grating layer is partially etched to implement a zero-contrast interface between the grating ridges and the sublayer, the local reflections and phase changes associated with hard interfaces is eliminated, thus the mirror effect of the HCG can be efficiently improved. In addition, from the point of view of fabrication, the sacrificial layer removal step in the HCG fabrication is not required for the ZCG fabrication, thus the whole device fabrication of the ZCG mirror can be highly simplified and the mechanical stability can be improved [16]. However, the leaky properties related with the resonant modes of the ZCG mirror has not been studied.

In this work, asymmetrical lateral leakage of light of a finite ZCG mirror is studied, and the dispersion equation of slab waveguide for the TM mode is proposed to analyze the resonant condition of the ZCG mirror. Two leaky channels are occurred in the reflection band due to the size effects of the ZCG and the excited source, where bound states in the continuums (BICs) turn into quasi-BICs as the angular component is nonzero. The resonant modes of the two leaky channels in short and long wavelengths are identified as the grating mode and sublayer mode, respectively; and they are all transferred into asymmetrical modes along the lateral direction from the center of the ZCG. The reflection reciprocity of the symmetrical system of the finite ZCG mirror can be broken due to the asymmetrical loss of the lateral leakage of light relative to incidence direction. By altering the excited source from the grating side to the sublayer side, the lateral leakage of light of the finite ZCG mirror can be highly reduced.

2. Simulation Model

Fig. 1(a) shows the schematic diagram of the infinite ZCG under the TM polarized plane wave illumination (magnetic-field vector lies along the y-axis). The refractive index of the ZCG is n, and the refractive indices of the cover and substrate region are n_c and n_s, respectively. Λ denotes the period of the ZCG, a is the width of the grating bar, d_g is the thickness of the grating ridge, d_h is the thickness of the sublayer, and θ is the angle of incidence. For the infinite ZCG, it means that the grating ridge is periodical in the x direction, and the incident wave is the plane wave. Fig. 1(b) denotes the calculation model of the finite ZCG, perfectly matched layer (PML) boundary conditions

are employed to describe the size effect, and the finite Gaussian source is placed at the center of the ZCG. The finite-difference time-domain (FDTD) method is adopted to calculate the spectral response of the finite ZCG [17].

For the infinite ZCG mirror, subwavelength structure is required so as to achieve high diffraction efficiency as light is incident from the grating side. That is

$$\Lambda < \frac{\lambda}{n_c \sin\theta + \max(n_c, n_s)}. \tag{1}$$

According to the effective media theory (EMT), the grating layer of the infinite ZCG mirror may be replaced by an equivalent anisotropic homogeneous medium, and the effective refractive index n_{eff} of the grating layer for TM mode can be approximated as [18]

$$n_{eff} = \left[\varepsilon_{0,TM} + \frac{\pi^2}{3} f^2 (1-f)^2 \left(\frac{1}{\varepsilon_H} - \frac{1}{\varepsilon_L} \right)^2 \varepsilon_{0,TM}^3 \varepsilon_{0,TE} \left(\frac{\Lambda}{\lambda} \right)^2 \right]^{\frac{1}{2}}, \tag{2}$$

where f is the grating filling factor with $f = a/\Lambda$; ε_H and ε_L are the relative permittivities of the grating materials with $\varepsilon_H = n^2$ and $\varepsilon_L = n_c^2$. $\varepsilon_{0,TM}$ and $\varepsilon_{0,TE}$ are the zero-order permittivities of the TM and TE modes, respectively. i.e.,

$$\varepsilon_{0,TE} = f\varepsilon_H + (1-f)\varepsilon_L, \tag{3}$$

$$\varepsilon_{0,TM} = \varepsilon_H \varepsilon_L / [f\varepsilon_L + (1-f)\varepsilon_H], \tag{4}$$

Since the infinite ZCG mirror can be equivalent to the thin-film structure in the subwavelength region, the ZCG structure can be taken as an equivalent ZCG waveguide. According to the slab waveguide theory [19], [20], the transverse magnetic field of the ZCG waveguide for the TM mode can be expressed as follows:

$$H_y(z) = \begin{cases} A_0 \exp(p_0 z), & -\infty < z < -d_h \\ A_1 \exp[i\kappa_1(z + d_h)] + B_1 \exp[-i\kappa_1(z + d_h)], & -d_h < z < 0 \\ A_2 \exp(i\kappa_2 z) + B_2 \exp(-i\kappa_2 z), & 0 < z < d_g \\ A_3 \exp[-p_1(z - d_g)], & d_g < z < +\infty \end{cases}, \tag{5}$$

where p_0, κ_1, κ_2, and p_1 are the wavenumbers of the substrate, the sublayer, the grating layer, and the cover in the z direction, respectively. Namely,

$$p_0 = (\beta^2 - k_0^2 n_s^2)^{1/2}, \tag{6}$$

$$\kappa_1 = (k_0^2 n^2 - \beta^2)^{1/2}, \tag{7}$$

$$\kappa_2 = (k_0^2 n_{eff}^2 - \beta^2)^{1/2}, \tag{8}$$

$$p_1 = (\beta^2 - k_0^2 n_c^2)^{1/2}, \tag{9}$$

where β is the propagation constant of the waveguide mode.

By using the transfer matrix method of slab waveguide [20], the eigenvalue equation of the matrix form for the ZCG waveguide can be immediately written as follows:

$$\begin{bmatrix} H_y(d_g) \\ \frac{1}{n_c^2} H_y(d_g) \end{bmatrix} = M_1 M_2 \begin{bmatrix} H_y(-d_h) \\ \frac{1}{n_s^2} H_y(-d_h) \end{bmatrix}, \tag{10}$$

where

$$M_1 = \begin{bmatrix} \cos(\kappa_1 d_h) & \frac{n^2}{\kappa_1} \sin(\kappa_1 d_h) \\ -\frac{\kappa_1}{n^2} \sin(\kappa_1 d_h) & \cos(\kappa_1 d_h) \end{bmatrix}, M_2 = \begin{bmatrix} \cos(\kappa_2 d_g) & \frac{n_{eff}^2}{\kappa_2} \sin(\kappa_2 d_g) \\ -\frac{\kappa_2}{n_{eff}^2} \sin(\kappa_2 d_g) & \cos(\kappa_2 d_g) \end{bmatrix}.$$

By using the continuity condition of H_y and $\partial H_y / \partial z$ at boundaries $z = -d_h$, $z = 0$, and $z = d_g$, the dispersion equation of the ZCG waveguide can be derived as:

$$\kappa_1 d_h = \upsilon\pi + \arctan\left(\frac{n^2 p_0}{n_s^2 \kappa_1}\right) + \arctan\left(\frac{n^2 p_2}{n_{eff}^2 \kappa_1}\right), \tag{11}$$

where $p_2 = \kappa_2 \tan[\tan^{-1}(\frac{p_1}{\kappa_2}) - \kappa_2 d_g]$, and υ is the order of waveguide mode.

To excite waveguide modes confined in the infinite ZCG mirror, the incident light has to satisfy the phase-matching condition of the ZCG waveguide, which will result in [21]

$$\beta \to \beta_m = k_0(n_c \sin\theta - m\lambda/\Lambda) \quad , m = \pm 1, \pm 2, \ldots. \tag{12}$$

where m is the diffraction order, k_0 is the wave vector in free space, and $k_0 = 2\pi/\lambda$. Combing Eqs. (11)–(12), the resonance locations between diffraction orders and waveguide modes of the infinite ZCG mirror can be estimated.

For the finite ZCG mirror, considering a Gaussian source of the form

$$E(x) = B \exp[-(x/w)]^2, \tag{13}$$

where w is the half-width of the field and B is a constant. The divergence angle θ' of the Gaussian source can be expressed as

$$\theta' = \frac{\lambda M^2}{\pi w}, \tag{14}$$

where M is the mode order of the Gaussian source. Because the refractive indices of the cover and the substrate are equal, the divergence angle θ' are identical for the same Gaussian source as the light incident from both the cover and substrate sides of the ZCG.

Taking the Fourier transform into consideration, the angular spectrum of the Gaussian source can be written as [22]

$$F(\theta', \lambda) = B'\pi b \exp(\pi w\theta'/\lambda)^2, \tag{15}$$

that is, the spectrum of the finite ZCG mirror under the Gaussian source illumination has nonzero angular components, and it can be approximated as the plane wave over the range of angles according to Eq. (15).

3. Results and Discussions

To clearly show the resonant condition of the ZCG mirror, the spectral properties of the ZCG and the resonance locations of the equivalent ZCG waveguide are investigated. As can be seen in Fig. 2(a), high-order resonant modes are occurred as the thickness of the sublayer is increased, and the refection response of the ZCG become more complicated due to the hybridization of multiple resonances, which is significantly different from those low-contrast gratings [23], [24]. In particular, in the near-wavelength regime, where the grating period is confined between the wavelengths inside the grating material and its surrounding media with $\lambda/n < \Lambda < \lambda$, mirror effect of the ZCG can be realized due to the overlapping of multiple resonant modes. Fig. 2(b) shows the estimated resonance locations of the ZCG using the dispersion relation of slab waveguide, and the equivalent ZCG waveguide structure is shown in the figure inset. Here, the order-mode resonance pair via the coupling between mth diffraction order and υ-order mode is denoted as $TM_{m,\upsilon}$. See Fig. 2(b), the estimated resonance locations of the equivalent ZCG waveguide approximately coincide with those of the ZCG. However, due to the approximation of the ZCG waveguide, there are slight discrepancies in resonance locations between the exact values and the estimated values. Although the resonant modes of the ZCG are mixed with each other in the near-wavelength regime, the location of each mode can be approximately predicted by combing with the dispersion curves of the ZCG waveguide.
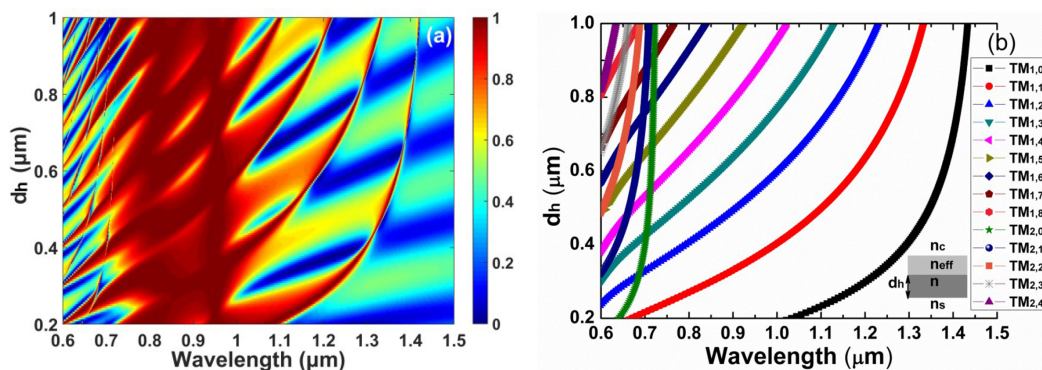
Fig. 2. Reflection properties and resonant locations of an infinite ZCG at normal incidence: $n_c = n_s = 1$, $n = 3.2$, $a = 0.214$ μm, $\Lambda = 0.454$ μm, and $d_g = 0.285$ μm. (a) Reflection d_h–λ map using the FDTD method. (b) Estimated resonance locations using the dispersion relation of slab waveguide.
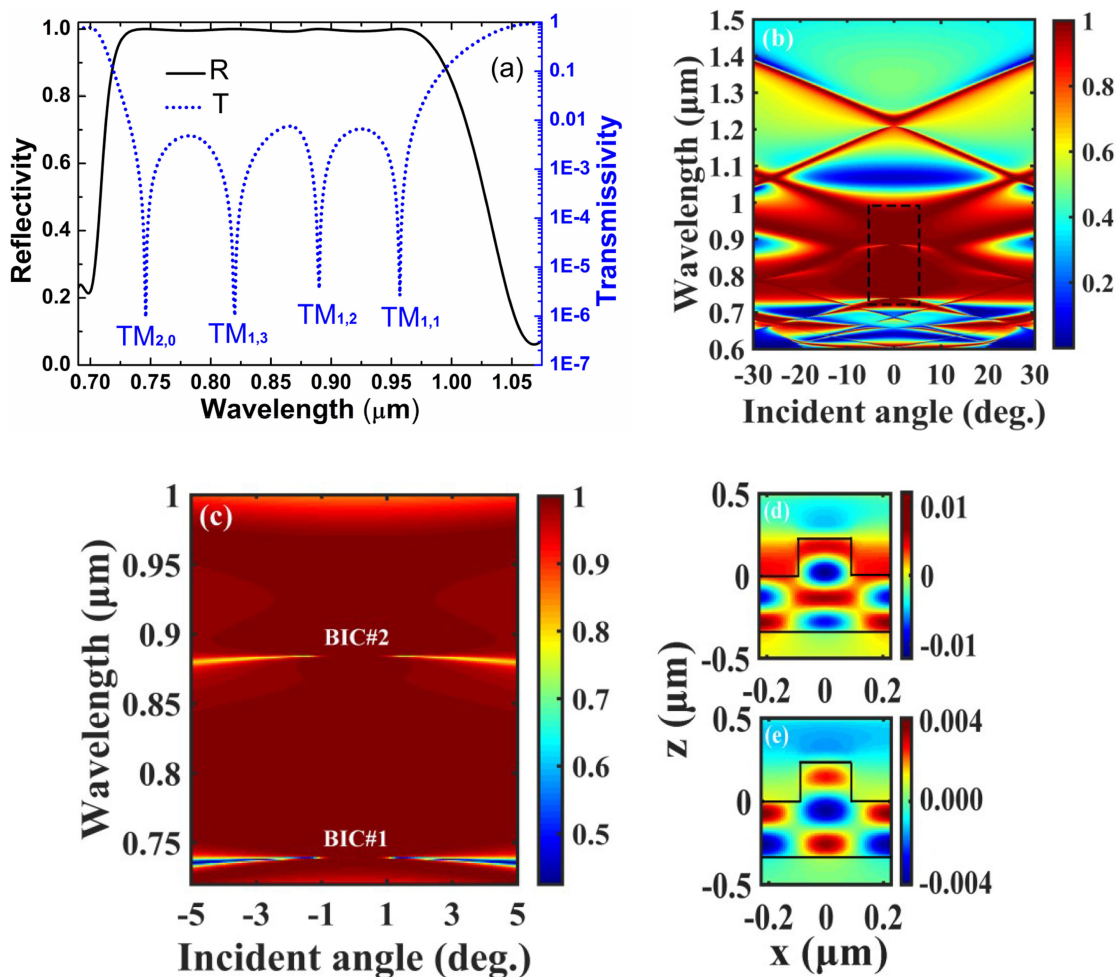

Fig. 3. Resonant properties of an infinite ZCG mirror: $n = 3.2$, $\Lambda = 0.454$ μm, $a = 0.214$ μm, $d_g = 0.285$ μm, and $d_h = 0.31$ μm. (a) Reflection and transmission spectra at normal incidence. (b) Reflection as functions of wavelength and incident angle. (c) Enlarged view of the dashed region in Fig. 3(b), (d), and (e) show the magnetic field profiles (H_y) for BIC#1 and BIC#2, respectively.

Fig. 3 shows the resonant properties of an infinite ZCG mirror under the TM wave illuminations, the structural parameters are the same as in Fig. 2(a) with $d_h = 0.31$ μm. As can be seen in Fig. 3(a), four order-mode resonance pairs of $TM_{2,0}$, $TM_{1,3}$, $TM_{1,2}$, and $TM_{1,1}$ are occurred in the reflection band of the ZCG mirror, which can be indicated by the transmission spectra in logarithmic scale [25]. The overlapping of these four resonant pairs create a wide reflection band ($\Delta\lambda/\lambda =$ 28.2%) with very high reflectivity (R > 99%). In Fig. 3(b), it can be seen that the resonant modes of the ZCG mirror split at oblique incidence, and every order-mode resonance pair splits into two branches of resonances due to the mode nondegeneracy [26], [27]. The mode degeneracy is broken as the incident light is deviated from the normal incidence, which permits interaction of the resulting differentiated modes with interesting consequences. Fig. 3(c) is the enlarged view of the dashed region in Fig. 3(b), where the incident angle is confined in a small angle range ($-5° \leq \theta \leq +5°$). As can be seen in Fig. 3(c), two leaky channels of the ZCG mirror disappear at zero in-plane wave vector ($k_{||} = 0$), which indicates the existence of two symmetry-protected BICs [28], [29], where leakage radiation to the surface normal direction is forbidden due to the conservation of the geometric symmetry of the ZCG [30], [31]. The two BICs of the ZCG with infinite Q factor are coexisting with the complete destructive interference of the resonant modes of $TM_{2,0}$, $TM_{1,3}$, $TM_{1,2}$, and $TM_{1,1}$; the wavelengths of BIC#1 and BIC#2 are 0.741 μm and 0.886 μm, respectively. Note the resonant locations of the two BICs almost do not shift as they turn into quasi-BICs with finite Q factor within a large incident angle range of $\pm5°$. As the incident angle is varied in the range of $\pm5°$, the locations of the two quasi-BICs in the shorter and longer wavelengths are almost kept the same at 0.74 μm and 0.88 μm, respectively. Unlike the HCG which supports only one symmetry-protected BIC mode [13], [27], [32], the ZCG mirror can support two symmetry-protected BIC modes due to the sublayer. In Figs. 3(d) and (e), we can see that the mode energy of BIC#1 is mainly confined in the grating layer, while the mode energy of the BIC#2 is mainly confined in the sublayer. The sublayer of the ZCG induces coupling between the grating modes and the waveguide modes, thus the range of frequency and angle with high reflectivity can be efficiently improved.

To study the size effect of the ZCG mirror, the size of the excited Gaussian source is fixed, and the ZCG size is varied. In Fig. 4, the lateral leakage is defined as 1-R-T with R and T as power reflectivity and transmissivity, respectively. As can be seen in Figs. 4(a) and (d), the reflection spectra are asymmetrical for the incidence from the grating side or the sublayer side, and two leaky channels are occurred at the wavelengths of 0.740 μm and 0.884 μm. The two leaky channels are resulted from the high-Q resonant modes, where the BICs turn into quasi-BICs as the angular component is nonzero. It is interesting to note that there are nonignorable leaky sidebands away from the two leaky channels, which are mainly resulted from the order-mode resonance pair. Unlike the narrowband grating reflector with finite size [33], whose lateral leakage of light is mainly resulted from guided-mode resonance, i.e., the order-mode resonance pairs; for the finite ZCG mirror, the lateral leakage of light of the quasi-BICs is dominant over that of the order-mode resonance pairs. In addition, the nonreciprocal reflection of the finite ZCG can be achieved even in the symmetrical system ($n_c = n_s$) due to the asymmetrical loss of the lateral leakage of light relative to incidence direction, which is different from those nanostructures where nonreciprocal reflection can be realized in the asymmetrical system ($n_c \neq n_s$) [34], [35]. According to Eq. (14), for the Gaussian source with a fixed size of 5 μm, its divergence angle can be calculated as 2.6°–4.0° within the wavelength region of 0.7–1.1 μm. It is obvious that the locations of the two quasi-BICs of the finite ZCG mirror are agree well with those of the infinite counterpart under oblique incidence as shown in Fig. 3(c).

In Figs. 4(b) and (e), it can be seen that the transmission spectra are identical for the incidences from both the grating side and the sublayer side. The transmission spectra are identical because they does not change under reversal of the structure due to the reciprocity theorem; however, reflection can be nonreciprocal if asymmetrical losses are incorporated in the structure. See Figs. 4(c) and (f), the lateral leakages are asymmetrical for the incidence from the grating side or the sublayer side. Since the transmission spectra are identical for both types of incidences, the asymmetrical reflection of the finite ZCG mirror is originated from the asymmetrical lateral leakage of light relative to incidence direction. In Fig. 4(g), ratio of peak lateral leakage is defined
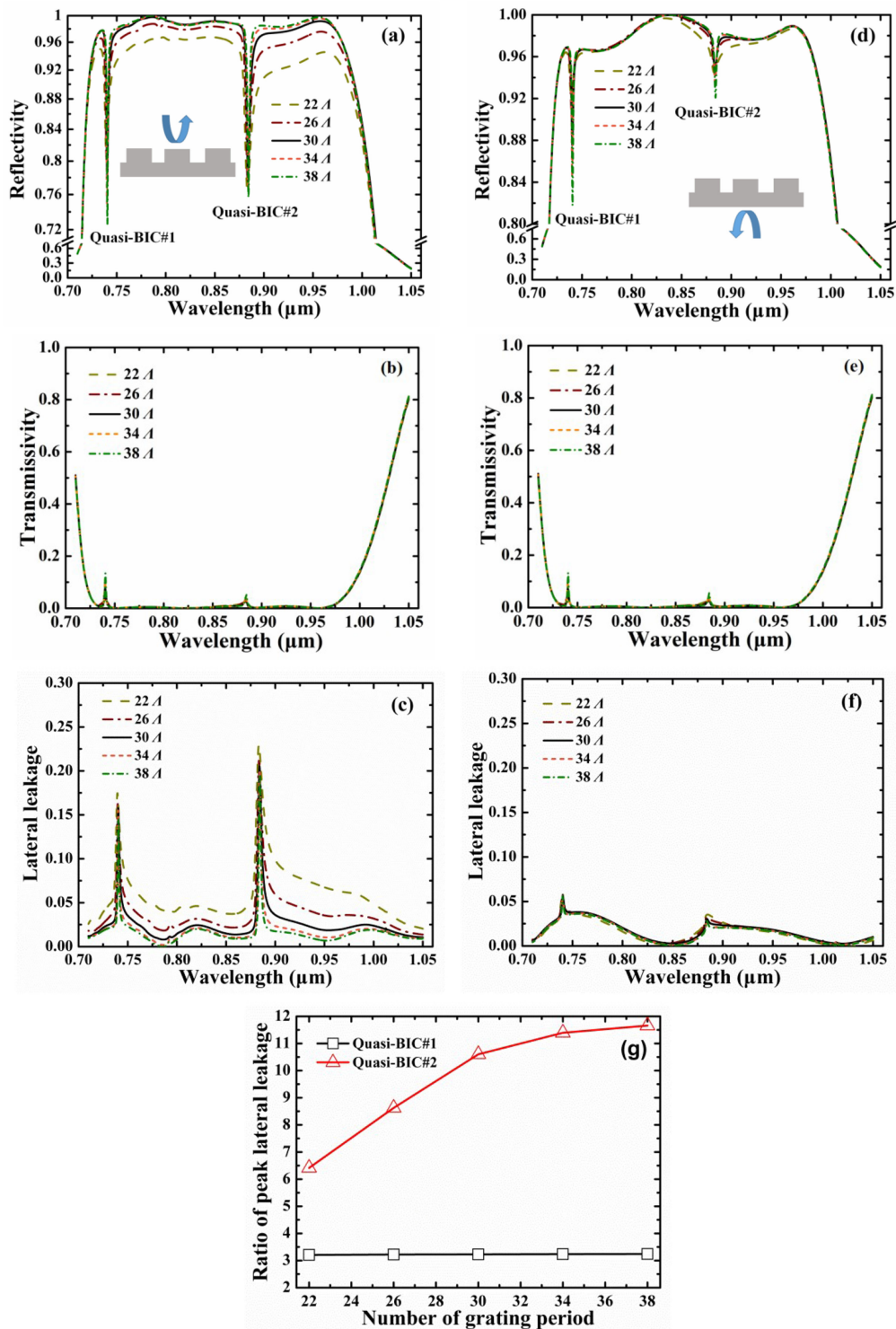
Fig. 4. Optical performances for different ZCG sizes with a fixed-size (5 μm, 1/e width of the Gaussian source) Gaussian source under normal incidence ($\theta = 0$). Here, $n = 3.2$, $\Lambda = 0.454$ μm, $a = 0.214$ μm, $d_g = 0.285$ μm, and $d_h = 0.31$ μm. (a), (b), and (c) are reflection, transmission, and lateral leakage for the incidence from the grating side, respectively. (d), (e), and (f) are reflection, transmission, and lateral leakage for the incidence from the sublayer side, respectively. (g) Ratio of peak lateral leakage as function of number of grating period for quasi-BIC#1 and quasi-BIC#2.
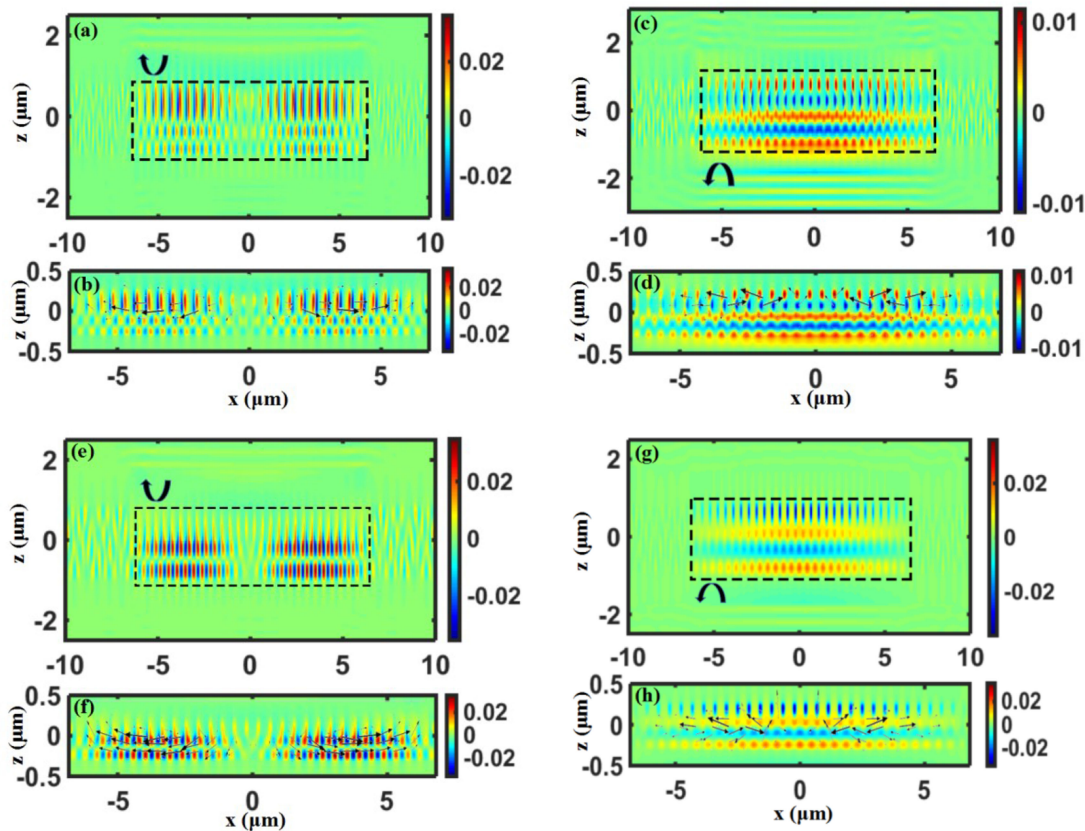
Fig. 5. Magnetic field profiles (H$_y$) and the energy flows (arrow maps) for the finite ZCG with 30Λ. Other parameters are the same as in Fig. 4 (a) H$_y$ distribution at 0.740 μm for the incidence from the grating side. (b) enlarged view of the region inside the dash line of (a). (c) H$_y$ distribution at 0.740 μm for the incidence from the sublayer side. (d) enlarged view of the region inside the dash line of (c). (e) H$_y$ distribution at 0.884 μm for the incidence from the grating side. (f) enlarged view of the region inside the dash line of (e). (g) H$_y$ distribution at 0.884 μm for the incidence from the sublayer side. (h) enlarge view of the region inside the dash line of (g).

as the ration between the peak values of the lateral leakage for the incidence from the grating side and the sublayer side. See Fig. 4(g), peak value of the lateral leakage of the finite ZCG mirror can be efficiently suppressed if the light is incident from the sublayer side. For the quasi-BIC#1, the ratio of peak lateral leakage is maintained at 3.2 as the number of the grating period is varied, while the ratio of peak lateral leakage of quasi-BIC#2 is increased with increasing the number of the grating period, and it increased to 11.7 as the number of the grating period is 38.

To understand the asymmetrical lateral leakage properties of the finite ZCG mirror, the field distributions and the energy flows are studied. As can be seen in Fig. 5, for both two types of incidences, the field profiles of H$_y$ are transformed from the symmetrical modes to the antisymmetrical modes from the center to the edges of the ZCG. The antisymmetrical mode has the odd symmetry with respect to the plane along the z direction, and it redirect the vertically incident wave into the in-plane direction (x direction), resulting in the lateral leakage of light. See Figs. 5(a) and (b), for the incidence from the grating side, the mode energy of the finite ZCG mirror is mainly confined in the grating layer for the quasi-BIC#1, and the leaky energy is mainly transferred from the center to the edges of the grating layer. However, see Figs. 5(c) and (d), for the incidence from the sublayer side, more mode energy is transferred into the sublayer, and a part of the leaky energy flows back as it propagates to the edges of the grating layer. As the light incident from the sublayer side, the incident wave can be diffracted back by the grating layer and can be recoupled into the leak modes
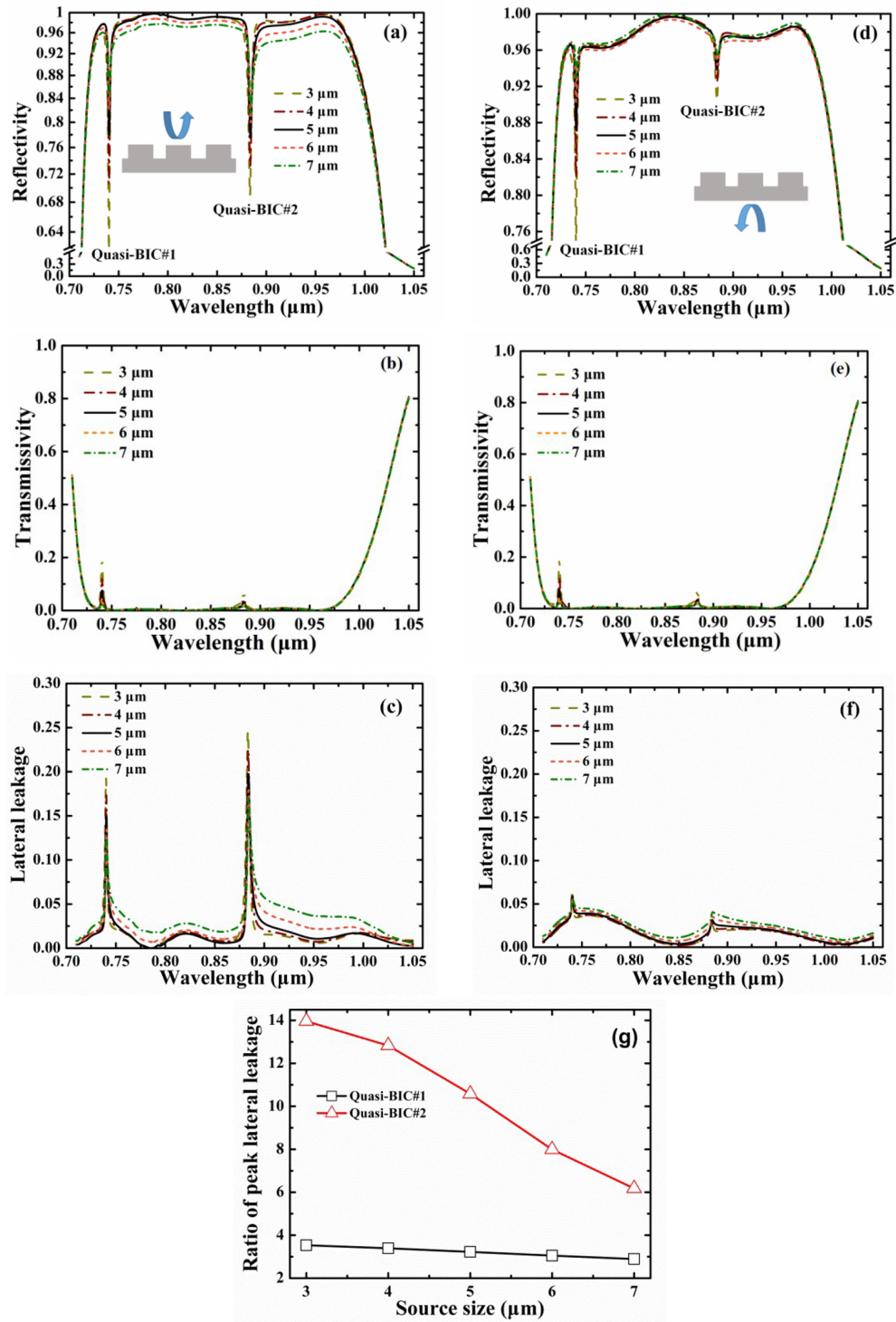
Fig. 6. Optical performances at different source sizes (1/e width of the Gaussian source) for a ZCG size of 30Λ. Here, $n = 3.2$, $\Lambda = 0.454$ μm, $a = 0.214$ μm, $d_g = 0.285$ μm, and $d_h = 0.31$ μm. (a), (b), and (c) are reflection, transmission, and lateral leakage for the incidence from the grating side, respectively. (d), (e), and (f) are reflection, transmission, and lateral leakage for the incidence from the sublayer side, respectively. (g) Ratio of peak lateral leakage as function of source size for quasi-BIC#1 and quasi-BIC#2.

[36], which may result in the backflowing of leaky wave. The backflowing energy reduces the lateral leakage of light, thus the lateral leakage of light can be highly suppressed comparing with that of the incidence from the grating side. In Figs. 5(e) and (f), for the incidence from the grating side, the mode energy of the finite ZCG mirror is mainly confined in the sublayer for the quasi-BIC#2, and the leaky energy is mainly transferred from the center to the edges in the sublayer; but for the incidence from the sublayer side, see Figs. 5(g) and (h), the lateral leakage of light can also be significantly reduced as the leaky energy is backflowed.

Fig. 6 shows optical properties at different source sizes for a 30Λ ZCG at normal incidence from both the grating side and the sublayer side. In Fig. 6(a), it can be seen that larger size of the Gaussian source results in the decrease of the reflectivity in the refection band. For the source size of 7 μm, the reflectivity in the reflection band is lower as compared to that of the source size of 3 μm due to the finite size effect of the ZCG. In addition, because the source size of 3 μm contains more nonzero angular components comparing with that of the source size of 7 μm, its reflection drops at the quasi-BIC wavelengths are deeper. In Figs. 6(b) and (c), it can be seen that the lateral leakages can be significantly altered as the source size is varied, but the transmission leakages are immune to the variation of the source size. In Figs. 6(d)–(f), it can be seen for the incidence from the sublayer side, although the transmission leakage is maintained at the same level as that of the incidence from the grating side, its lateral leakage can also be significantly reduced. See Fig. 6(g), for the quasi-BIC#1, the ratio of peak lateral leakage is kept around 3.0 as the size of the Gaussian source is varied; for the quasi-BIC#2, although the ratio of peak lateral leakage is decreased with the increase of the size of Gaussian source, the ratio of peak lateral leakage is high than 6.1 as the source size is increased to 7 μm.

4. Conclusion

The asymmetrical lateral leakage of light in a finite ZCG mirror is numerically demonstrated. The dispersion equation of slab waveguide for the TM mode is proposed to evaluate the resonant condition of the ZCG mirror, it is shown that the mirror effect of the infinite ZCG is resulted from the overlapping of order-mode resonance pairs. However, two leaky channels are occurred in the spectra of the finite ZCG mirror for the normal-incident Gaussian source. The two leaky channels are resulted from the high-Q resonant modes, where two BICs turn into two quasi-BICs as the angular component of the incident wave is nonzero. The resonant modes of the two leaky channels in short and long wavelengths are identified as the grating mode and sublayer mode, respectively; and they are all transferred into asymmetrical modes along the lateral direction from the center of the ZCG. The reflection reciprocity of the symmetrical system of the finite ZCG mirror can be broken due to the asymmetrical loss of the lateral leakage of light. By changing the excited source from the grating side to the sublayer side, the lateral leakage of light of the finite ZCG mirror can be highly reduced with the backflowing of the leaky mode. The asymmetrical lateral leakage of light relative to incidence direction provide a general knowledge for designing practical grating mirrors in various applications such as lasers, sensors, and switches.

References

[1] H. A. Macleod, *Thin-Film Opticalfilter*, 3rd ed. New York, NY, USA: McGraw-Hill, 2001.
[2] C. F. R. Mateus, M. C. Y. Huang, L. Chen L, C. J. Chang-Hasnain, and Y. Suzuki, "Broad-band mirror (1.12–1.62 μm) using a subwavelength grating," *IEEE Photon. Technol. Lett.*, vol. 16, no. 7, pp. 1676–1678, Jul. 2004.
[3] V. Karagodsky and C. J. Chang-Hasnain, "Physics of near-wavelength high contrast gratings," *Opt. Exp.*, vol. 20, no. 10, pp. 10888–10895, May 2012.
[4] C. J. Chang-Hasnain and W. Yang, "High contrast gratings for integrated optoelectronics," *Adv. Opt. Photon.*, vol. 4, no. 3, pp. 379–440, Sep. 2012.
[5] M. Marciniak *et al.*, "Optimal parameters of monolithic high-contrast grating mirrors," *Opt. Lett.*, vol. 41, no. 15, pp. 3495–3498, Aug. 2016.
[6] L. Huang, D. Liang, J. Zeng, Y. Xiao, H. Wu, and W. Xiao, "SOI-based high performance multi-subpart profile grating mirror," *Opt. Laser Technol.*, vol. 78, pp. 1–4, Apr. 2016.
[7] D. A. Bekele, G. C. Park, R. Malureanu, and I.-S. Chung, "Polarization-independent wideband high-index-contrast grating mirror," *IEEE Photon. Technol. Lett.*, vol. 27, no. 16, pp. 1733–1736, Aug. 2015.

[8] K. Ikeda, K. Takeuchi, K. Takayose, Il.-S. Chung, J. Mørk, and H. Kawaguchi, "Polarization-independent high-index contrast grating and its fabrication tolerances," *Appl. Opt.*, vol. 52, no. 5, pp. 1049–1053, Feb. 2013.

[9] M. Gębski *et al.*, "Transverse mode control in high-contrast grating VCSELs," *Opt. Exp.*, vol. 22, no. 17, pp. 20954–20963, Aug. 2014.

[10] T. Sun, S. Kan, G. Marriott, and C. Chang-Hasnain, "High-contrast grating resonators for label-free detection of disease biomarkers," *Sci. Rep.*, vol. 6, Jun. 2016, Art. no. 27482.

[11] A. Liu, H. E. Hofmann, and D. H. Bimberg, "Integrated high-contrast-grating optical sensor using guided mode," *IEEE J. Quantum Electron.*, vol. 51, no. 1, Jan. 2015, Art. no. 6600108.

[12] Z. Wang *et al.*, "Mode splitting in high-index-contrast grating with mini-scale finite size," *Opt. Lett.*, vol. 41, no. 16, pp. 3872–3875, Aug. 2016.

[13] A. Liu, W. Hofmann, and D. Bimberg, "Two dimensional analysis of finite size high-contrast gratings for applications in VCSELs," *Opt. Exp.*, vol. 22, no. 10, pp. 11804–10811, May. 2014.

[14] R. Magnusson, "Wideband reflectors with zero-contrast gratings," *Opt. Lett.*, vol. 39, no. 15, pp. 4337–4340, Aug. 2014.

[15] M. Shokooh-Saremi and R. Magnusson, "Properties of two-dimensional resonant reflectors with zero-contrast gratings," *Opt. Lett.*, vol. 39, no. 24, pp. 6958–6961, Dec. 2014.

[16] A. Liu, W. Zheng, and D. Bimbergc, "Comparison between high- and zero-contrast gratings as VCSEL mirrors," *Opt. Commun.*, vol. 389, pp. 35–41, Apr. 2017.

[17] FDTD Solutions, [Online]. Available: https://www.lumerical.com

[18] S. M. Rytov, "Electromagnetic properties of a finely stratified medium," *Sov. Phys. J. Exp. Theor. Phys.*, vol. 2, pp. 466–475, 1956.

[19] D. Marcuse, *Theory of Dielectric Optical Waveguide*, 2nd ed. New York, NY, USA: Academic, 1974.

[20] X. Wang, C. Yin, and Z. Cao, *Progress in Planar Optical Waveguides*. Shanghai, China: Shanghai Jiao Tong University Press, 2016.

[21] Y. Ding and R. Magnusson, "Doubly resonant single-layer bandpass optical filters," *Opt. Lett.*, vol. 29, no. 10, pp. 1135–1137, May. 2004.

[22] D. W. Peters, S. A. Kemme, and G. R. Hadley, "Effect of finite grating, waveguide width, and end-facet geometry on resonant subwavelength grating reflectivity," *J. Opt. Soc. Amer. A*, vol. 21, no. 6, pp. 981–987, Jun. 2004.

[23] L. Qian, D. Zhang, C. Tao, R. Hong, and S. Zhuang, "Tunable guided-mode resonant filter with wedged waveguide layer fabricated by masked ion beam etching," *Opt. Lett.*, vol. 41, no. 5, pp. 982–985, Mar. 2016.

[24] J. Zhou *et al.*, "Modal analysis on resonant excitation of two-dimensional waveguide grating filters," *Opt. Commun.*, vol. 405, pp. 350–354, Dec. 2017.

[25] T. Sang, L. Wang, S. Ji, Y. Ji, H. Chen, and Z. Wang, "Systematic study of the mirror effect in a poly-Si subwavelength periodic membrane," *J Opt. Soc. Am. A*, vol. 26, no. 3, pp. 559–565, Mar. 2009.

[26] T. Sang, Z. Wang, L. Wang, Y. Wu, and L. Chen, "Resonant excitation analysis of sub-wavelength dielectric grating," *J. Opt. A: Pure Appl. Opt.*, vol. 8, no. 1, pp. 62–66, Jan. 2006.

[27] S. Han, M. V. Rybin, P. Pitchappa, Y. K. Srivastava, Y. S. Kivshar, and R. Singh, "Guided-mode resonances in all-dielectric terahertz metasurfaces," *Adv. Opt. Mater.*, vol. 8, Sep. 2019, Art. no. 1900959.

[28] J. M. Foley and J. D. Phillips, "Normal incidence narrowband transmission filtering capabilities using symmetry-protected modes of a subwavelength, dielectric grating," *Opt. Lett.*, vol. 40, no. 11, pp. 2637–2740, Jun. 2015.

[29] C. W. Hsu, B. Zhen, A. D. Stone, J. D. Joannopoulos, and M. Soljačić, "Bound states in the continuum," *Nat. Rev. Mater.*, vol. 1, no. 9, Sep. 2016, Art. no. 6600108.

[30] J. Lee *et al.*, "Observation and differentiation of unique high-Q optical resonances near zero wave vector in macroscopic photonic crystal slabs," *Phys. Rev. Lett.*, vol. 109, no. 6, Aug. 2012, Art. no. 067401.

[31] A. Kodigala, T. Lepetit, Q. Gu, B. Bahari, Y. Fainman, and B. Kantć, "Lasing action from photonic bound states in continuum," *Nature*, vol. 541, no. 7636, pp. 196–199, Jan. 2017.

[32] J. W. Yoon, S. H. Song, and R. Magnusson, "Critical field enhancement of asymptotic optical bound states in the continuum," *Sci. Rep.*, vol. 5, Dec. 2015, Art. no. 18301.

[33] A. Szczepkowicz, "Guided-mode resonance, resonant grating thickness, and finite-size effects in dielectric laser acceleration structures," *Appl. Opt.*, vol. 55, no. 10, pp. 2634–2638, Apr. 2016.

[34] E. Altewischer, M. P. van Exter, and J. P. Woerdman, "Nonreciprocal reflection of a subwavelength hole array," *Opt. Lett.*, vol. 28, no. 20, pp. 1906–1908, Oct. 2003.

[35] J. W. Yoon, and R. Magnusson, "Fano resonance formula for lossy two-port systems," *Opt. Exp.*, vol. 21, no. 15, pp. 17751–17759, Jul. 2013.

[36] T. Sang *et al.*, "Tunable optical reflectance using a monolithic encapsulated grating," *Opt. Laser Technol.*, vol. 83, pp. 163–167, Sep. 2016.